AIAA JOURNAL
Vol. 34, No. 1, January 1996

Numerical Simulation of Mixing for Turbulent Slot Injection

P. Gerlinger,* J. Algermissen,† and D. Brüggemann†
University of Stuttgart, 70550 Stuttgart, Germany

Flowfields are simulated that are induced by sonic jets injected into supersonic airstreams. Results on structure and mixing of such jets are presented. Several two-dimensional cases are treated using a low-Reynolds-number q-ω turbulence model. The influence of some turbulence modeling corrections and of artificial dissipation are investigated for flat plate test cases where nitrogen is injected transversely into the supersonic airstream. The results demonstrate the necessity to use modeling corrections and to reduce artificial viscosity in near-wall regions. The numerical code is also used to calculate a similar transverse helium injection into a ducted airstream. In a further investigation hydrogen is injected axially into the mainstream. In this case mixing is strongly influenced by turbulent diffusion. Pressure and species profiles are compared with experimental data.

Nomenclature

$C_{\omega 1}$ = low-Reynolds-number function
c = speed of sound, m/s
D = divergence of the velocity field, m/s
D_q = low-Reynolds-number damping function
E = total specific energy, m^2/s^2
$\boldsymbol{F}, \boldsymbol{G}$ = flux vector in x, y direction, respectively
h_i = specific enthalpy of species i, J/kg
k = turbulent kinetic energy, m^2/s^2
l_t = turbulent length scale, m
l_W = nearest wall distance to a volume center, m
M_t = turbulent Mach number, $(\sqrt{2q}/c)$
N_k = number of different species
p, p_t = static, total pressure, respectively, N/m^2
$\boldsymbol{Q}$ = conservative variable vector
q = turbulence transport variable, $(\sqrt{k})$, m/s
q_x, q_y = heat flux, W/m^2
R_q = turbulent Reynolds number
$\boldsymbol{S}$ = source vector
S = strain invariant, $1/s^2$
Tu = turbulence intensity
t = time, s
u, v = velocity components, m/s
$\tilde{u}_i, \tilde{v}_i$ = diffusion velocities of species i, m/s
w_{ref} = absolute reference velocity, m/s
X_i = mole fraction of species i
x, y = Cartesian coordinates
Y_i = mass fraction of species i
y^+ = nondimensional wall distance
ϵ = dissipation rate of k, m^2/s^3
μ = viscosity, kg/(ms)
ρ = density, kg/m^3
τ = stress tensor, $kg/(ms^2)$
ω = turbulence transport variable, (ϵ/k), 1/s

Subscripts

inj = injected
m = molecular
n = normal to the wall
t = turbulent
v = viscous flux
∞ = freestream

Presented as Paper 94-2247 at the AIAA 25th Fluid Dynamics Conference, Colorado Springs, CO, June 20–23, 1994; received July 22, 1994; revision received Jan. 23, 1995; accepted for publication March 6, 1995.

*Research Scientist, Department of Aerospace Engineering, Pfaffenwaldring 31. Member AIAA.
†Professor, Department of Aerospace Engineering, Pfaffenwaldring 31.

Introduction

WITH growing interest in supersonic combustion, an accurate simulation of the turbulent injection and mixing process of gaseous fuel into a supersonic airstream became very important. The complicated physics of such flowfields cause the modeled equations, governing turbulence, to become mathematically stiff, making numerical solutions difficult. An exact modeling of the injection process, including separation in front and behind of the injector, requires the integration of the turbulence model directly to a solid boundary. However, near-wall corrections for low-Reynolds-number models often lack in robustness. All results of this paper are obtained using a low-Reynolds-number q-ω turbulence closure.[1] In previous investigations,[2] we also employed a low-Reynolds-number k-ϵ model in a version of Launder and Sharma.[3] For wall slot injections at high pressure ratios the q-ω model was found to be superior to the k-ϵ model because of its high numerical stability, which enables convergence even in cases where we failed with the k-ϵ closure. A second very important advantage of the q-ω model is the option for stationary flows to initialize the turbulent flowfield with constant freestream values. With this technique, solutions are obtained even in cases with injection, massive separation, and shock-wave/boundary-layer interaction.

Governing Equations

The two-dimensional, averaged Navier–Stokes and species transport equations for a multicomponent gas are given by

$$\frac{\partial \boldsymbol{Q}}{\partial t} + \frac{\partial (\boldsymbol{F} - \boldsymbol{F}_v)}{\partial x} + \frac{\partial (\boldsymbol{G} - \boldsymbol{G}_v)}{\partial y} = 0 \tag{1}$$

where

$$\boldsymbol{Q} = [\rho,\ \rho u,\ \rho v,\ \rho E,\ \rho Y_j]^t \tag{2}$$

$$\boldsymbol{F} = \begin{bmatrix} \rho u \\ \rho u^2 + p \\ \rho uv \\ u(\rho E + p) \\ \rho u Y_j \end{bmatrix}, \qquad \boldsymbol{F}_v = \begin{bmatrix} 0 \\ \tau_{xx} \\ \tau_{xy} \\ u\tau_{xx} + v\tau_{xy} - q_x \\ -\rho \tilde{u}_j Y_j \end{bmatrix} \tag{3}$$

$$\boldsymbol{G} = \begin{bmatrix} \rho v \\ \rho uv \\ \rho v^2 + p \\ v(\rho E + p) \\ \rho v Y_j \end{bmatrix}, \qquad \boldsymbol{G}_v = \begin{bmatrix} 0 \\ \tau_{xy} \\ \tau_{yy} \\ u\tau_{xy} + v\tau_{yy} - q_y \\ -\rho \tilde{v}_j Y_j \end{bmatrix} \tag{4}$$

and $j = 1, 2, \ldots, N_k - 1$. Note that a contribution from turbulence is included in

$$E = \sum_{j=1}^{N_k} Y_j h_j - \frac{p}{\rho} + \frac{1}{2}(u^2 + v^2) + q^2 \tag{5}$$

Using a Boussinesq approximation, we get

$$\tau_{xy} = \mu \left(\frac{\partial u}{\partial y} + \frac{\partial v}{\partial x} \right) \tag{6}$$

$$\tau_{xx} = 2\mu \frac{\partial u}{\partial x} - 2/3\mu \left(\frac{\partial u}{\partial x} + \frac{\partial v}{\partial y} \right) - 2/3\rho k \tag{7}$$

$$\tau_{yy} = 2\mu \frac{\partial v}{\partial y} - 2/3\mu \left(\frac{\partial u}{\partial x} + \frac{\partial v}{\partial y} \right) - 2/3\rho k \tag{8}$$

where $\mu = \mu_m + \mu_t$ is the sum of the molecular and turbulent (eddy) viscosities. In the same way the conductivity and diffusivities of the gas are formed by a molecular and turbulent part using constant turbulent Prandtl and Schmidt numbers[4] of 0.9.

Numerical Method

For solving the governing equations as well as the turbulence transport equations an implicit lower-upper symmetric Gauss–Seidel (LU-SGS) method[4,5] in finite volume formulation is employed. For high-Reynolds-number flows it is often sufficient to use only the inviscid Jacobians in the implicit operator to integrate the full Navier–Stokes equations in time. However, low-Reynolds-number turbulence closures require very fine grids near solid walls. There and within separated regions the flow is often dominated by viscous effects, and it is advantageous to add viscous Jacobians in the implicit operator. This is done in a simplified form based on the thin-layer Navier–Stokes equations.[2,6] The integration of the turbulence transport equations is done in a decoupled way from the fluid motion because no improvements could be achieved in case of a coupling. Therefore we first integrate the mean flow equations in time with frozen values of q and ω and in a next step integrate the turbulence equations with frozen mean flow values. As it is often complicated to transform a flow problem using one single grid, the complete code is held in a block structured form.

Artificial Viscosity

For the right-hand side (RHS) discretization we use central differences. Therefore we need some kind of artificial viscosity to reduce oscillations near shocks and enable convergence to machine accuracy. Usually this is a blend of second and fourth differences, originally developed by Jameson et al.,[7] where the artificial dissipation is scaled by the spectral radius of the concerning flux Jacobian. Recently Turkel[8] and Swanson[9] introduced a matrix dissipation for the Navier–Stokes equations that permits reducing the amount of artificial dissipation by scaling each equation individually. We have extended this procedure to multicomponent flow.[10] All results presented in this paper are calculated using a matrix dissipation. With a special sensor and correct parameters the second-order scheme becomes first order upwind near shocks and gets total variation diminishing (TVD) properties.[9] A free parameter is used to blend over between the original non-TVD and the more dissipative TVD sensor, both based on the pressure. The amount of added artificial dissipation may also have an influence on the spread of separated regions. Because of the highly stretched grids near solid walls we used an anisotropic scaling. Additionally, the scaling functions are multiplied by a normalized local relative velocity, $\sqrt{(u^2 + v^2)}/w_{\text{ref}}$, to reduce artificial viscosity in the near-wall regions.[10] Otherwise artificial viscosity can contaminate the physical dissipation.[11]

q-ω Turbulence Model

The q-ω low-Reynolds-number turbulence model was first presented in 1983 by Coakley[12] and was modified several times.[1,13,14] For the calculations presented in this paper a 1992 version[1] was used. Although the high-Reynolds-number constants for the first version are obtained from corresponding constants in the k-ϵ model, the constants for the latest version are based on the k-ω^2 model.[13] The turbulent transport variables are $q = \sqrt{k}$ and $\omega = \epsilon/k$. The field equations for these variables are written as

$$\frac{\partial \boldsymbol{Q}_{q\omega}}{\partial t} + \frac{\partial \left(\boldsymbol{F}_{q\omega} - \boldsymbol{F}_{q\omega_v} \right)}{\partial x} + \frac{\partial \left(\boldsymbol{G}_{q\omega} - \boldsymbol{G}_{q\omega_v} \right)}{\partial y} = \boldsymbol{S}_{q\omega} \tag{9}$$

where

$$\boldsymbol{Q}_{q\omega} \begin{bmatrix} \rho q \\ \rho \omega \end{bmatrix} \qquad \boldsymbol{F}_{q\omega} = \begin{bmatrix} \rho u q \\ \rho u \omega \end{bmatrix} \qquad \boldsymbol{G}_{q\omega} = \begin{bmatrix} \rho v q \\ \rho v \omega \end{bmatrix} \tag{10}$$

$$\boldsymbol{F}_{q\omega_v} = \begin{bmatrix} \left(\mu_m + \dfrac{\mu_t}{\sigma_q} \right) \dfrac{\partial q}{\partial x} \\ \left(\mu_m + \dfrac{\mu_t}{\sigma_\omega} \right) \dfrac{\partial \omega}{\partial x} \end{bmatrix} \qquad \boldsymbol{G}_{q\omega_v} = \begin{bmatrix} \left(\mu_m + \dfrac{\mu_t}{\sigma_q} \right) \dfrac{\partial q}{\partial y} \\ \left(\mu_m + \dfrac{\mu_t}{\sigma_\omega} \right) \dfrac{\partial \omega}{\partial y} \end{bmatrix} \tag{11}$$

$$\boldsymbol{S}_{q\omega} = \begin{bmatrix} C_{q1} \left(C_\mu D_q \dfrac{S}{\omega^2} - \dfrac{2}{3} \dfrac{D}{\omega} - 1 \right) \rho \omega q \\ \left[C_{\omega 1} \left(C_\mu \dfrac{S}{\omega^2} - C_{\omega 3} \dfrac{D}{\omega} \right) - C_{\omega 2} \right] \rho \omega^2 \end{bmatrix} \tag{12}$$

With the strain invariant defined by

$$S = \left[2\frac{\partial u}{\partial x} - \frac{2}{3} \left(\frac{\partial u}{\partial x} + \frac{\partial v}{\partial y} \right) \right] \frac{\partial u}{\partial x} + \left(\frac{\partial u}{\partial y} + \frac{\partial v}{\partial x} \right)^2 + \left[2\frac{\partial v}{\partial y} - \frac{2}{3} \left(\frac{\partial u}{\partial x} + \frac{\partial v}{\partial y} \right) \right] \frac{\partial v}{\partial y} \tag{13}$$

and the divergence of the velocity field

$$D = \frac{\partial u}{\partial x} + \frac{\partial v}{\partial y} \tag{14}$$

we get the production rate of turbulent kinetic energy $P_k = \mu_t S - (2/3)\rho k D$. For modeling the low-Reynolds-number regions Coakley and Huang[1] introduced the damper D_q and the function $C_{\omega 1}$

$$D_q = 1 - \exp(-0.022 R_q), \qquad C_{\omega 1} = 0.5 D_q + 0.055 \tag{15}$$

which depend on the turbulent Reynolds number

$$R_q = \frac{\rho q l_W}{\mu} \tag{16}$$

The basic constants of this model are

$$\begin{aligned} C_{q1} &= 0.5, & C_{\omega 2} &= 0.833, & C_{\omega 3} &= 2/3 \\ \sigma_q &= 0.8, & \sigma_\omega &= 2.0, & C_\mu &= 0.09 \end{aligned} \tag{17}$$

Finally the eddy viscosity is calculated by

$$\mu_t = C_\mu D_q \frac{\rho q^2}{\omega} \tag{18}$$

The boundary conditions at solid walls are $q = 0$ and $\partial\omega/\partial n = 0$, and the freestream and inflow conditions are taken from Ref. 1, using a characteristic length. At the injection slot fixed values for q and ω are specified. As the production term near the injector and not the convective transport through the jet dominates the behavior, the solution is not very sensitive to a variation of these values.

The preceding equations describe the standard q-ω turbulence model. For cases with slot injection we investigated possible improvements by the introduction of some modeling corrections.

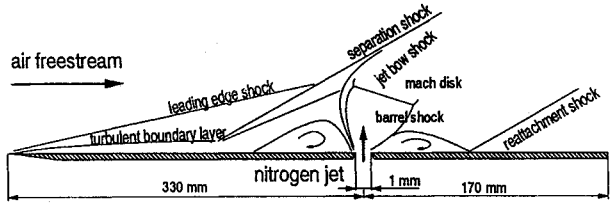

Fig. 1 Geometry and flowfield characteristics.

Correction 1

To improve the prediction of the surface heat transfer, a limitation on the turbulent length scale l_t was introduced in Ref. 1 (here for $y^+ \leq 20$). We use this as a constraint of the variable ω

$$l_t = \min(2.5 l_w,\ q/\omega), \qquad \omega = q/l_t \tag{19}$$

This modification has only a small influence on skin friction and separation.

Correction 2

Vuong and Coakley[14] investigated the q-ω turbulence model for an oblique shock-wave and boundary-layer interaction flow. Here the standard model can be strongly improved by a compressibility correction that results in an increase of the separation bubble size. This correction leads to a new constant for the velocity divergence term, which now becomes

$$C_{\omega 3} = 2.4 \tag{20}$$

and is derived for uniaxial compression. This correction has a stronger influence than correction 1. Both modifications do not affect the performance of the model for attached flows.[1]

Correction 3

This compressibility correction was first introduced by Sarkar et al.[15] for the k-ϵ model to correct compressible mixing layers in comparison to incompressible ones. Rizzetta[16] used this correction for air wall injections and obtained an improvement in the magnitude of peak pressure and the extension of the jet interaction region. We transformed this correction directly to the q-ω model. It appears in the source term of the q equation where the term -1 within the brackets has to be replaced by

$$-\left(1 + \alpha M_t^2\right) \tag{21}$$

The constant α was taken as 1 as suggested by Sarkar et al.[15]

Results

Three different test cases with transverse (N_2, He) and axial (H_2) slot injection have been investigated.

Experiment of Aso et al.

Aso et al.[17] investigated experimentally a nitrogen secondary flow injected into a supersonic airstream. These investigations were performed for different total pressure ratios between the injected stream and the main flow. Figure 1 shows the flowfield characteristics and the geometry. The computational grid consisted of 301 × 69 grid points. With the exception of the first grid points in the immediate vicinity of the leading edge, we obtained values for $y^+ \leq 0.23$ for the first grid points away from the wall. The mesh spacing near solid walls is critical for low-Reynolds-number models. Investigations[1] have shown an increased error in skin friction for $y^+ \geq 1$. We have refined the grid near the wall, the injection slot, and the leading edge and increased the number of grid points in comparison with previous calculations[2] to get a grid-independent solution. The air mainstream has a Reynolds number of 2.07×10^7 based on the length $l = 0.33$ m from the leading edge to the injection slot and a Mach number of 3.71. The total temperature and total pressure are 301 K and 12 bar, respectively. The total temperature of the sonically injected nitrogen is 301 K. Three different total pressure ratios ($p_{t,\mathrm{inj}}/p_{t,\infty} = 0.31$, 0.42, and 0.49) are investigated numerically. The slot width of 1 mm

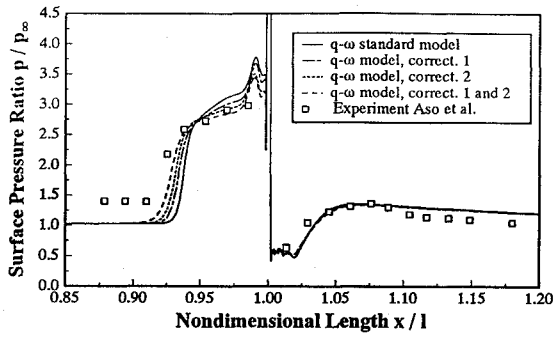

Fig. 2 Surface static pressure distributions for the standard q-ω model and corrected versions.

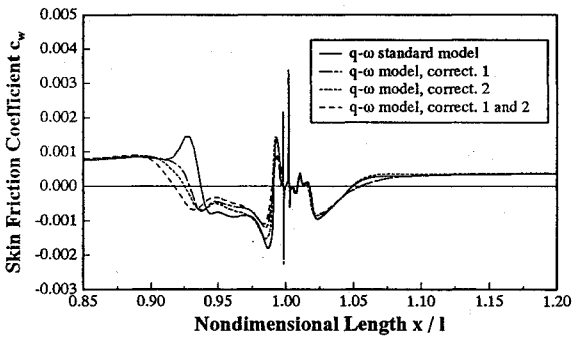

Fig. 3 Skin-friction distributions for the standard q-ω model and corrected versions.

is resolved by 20 cells. For the total pressure ratio of 0.31 we investigated the influence of the described modeling corrections. Figure 2 shows the nondimensional static surface pressure distributions near the injection slot for calculations with and without corrections. We observed the same effect as Coakley and Hsieh[13] for oblique shock-wave and boundary-layer interaction flow: the standard q-ω model fails to predict the separation correctly. The size of separation in front of the injector is strongly underpredicted. Improvements are obtained by the described modeling corrections. Best agreement with the experiment is achieved if corrections 1 and 2 are used combined. Although the size of separation increases, the peak pressure is lowered and in better correspondence with experimental results. The modifications of the standard model have nearly no influence on the pressure distribution downstream of the injector. Within the skin friction distribution, shown in Fig. 3, a small change downstream of the injector is obtained if correction 1 is used. In front of the jet-induced separation the standard q-ω model has an unrealistic overshoot that disappears if the corrections are applied. Similar results are obtained if correction 3 is used. Figures 4 and 5 show a comparison using corrections 1 and 2 or correction 3. Because of the somewhat better agreement with the experiment, corrections 1 and 2 are used for all following calculations.

Further calculations are performed to demonstrate the effect of added artificial viscosity. The employed second- and fourth-order dissipation is ruled by a sensor that is normally based on the static pressure. This sensor locates shock waves within the flowfield where the second-order dissipation is needed to suppress oscillations. Wallin and Gronland[18] used the pressure as switch parameter for the mean flow variables and the turbulent kinetic energy for the turbulence transport equations. With this strategy we obtained worse results for the test case described. Because of the strong gradients within the k distribution near the injector, such a treatment led to strong oscillations. Therefore all results presented are obtained using a single pressure-based switch. For a further reduction of artifical viscosity this term is additionally multiplied with $(\sqrt{u^2 + v^2}/w_{\mathrm{ref}})^\beta$. This is necessary because near solid walls or within separated regions very strong gradients in some flow variables may exist. In this case the second- and fourth-order derivatives can be quite large, often leading to large nonphysical values of artificial dissipation.[10,11] The reference relative velocity scale w_{ref} is chosen to be the freestream velocity and β is taken to be 1.

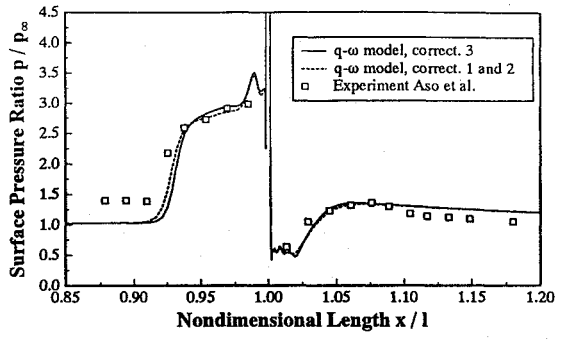

Fig. 4 Surface static pressure distributions for corrected versions of the q-ω model.

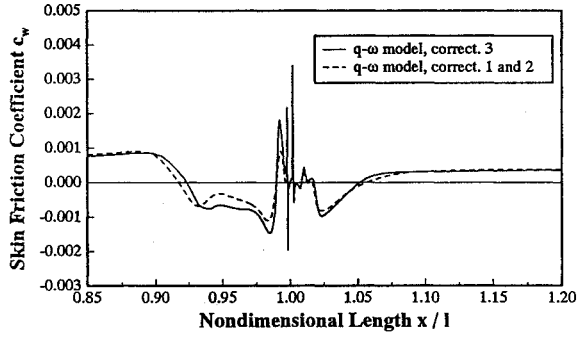

Fig. 5 Skin-friction distributions for corrected versions of the q-ω model.

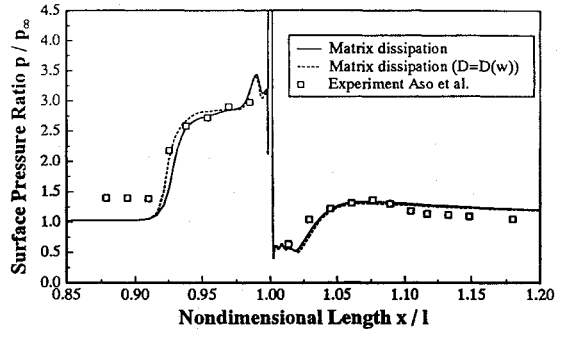

Fig. 6 Surface static pressure distributions for different kinds of artificial dissipation scaling.

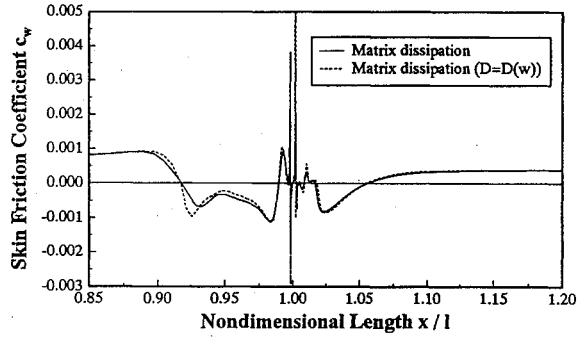

Fig. 7 Skin-friction distributions for different kinds of artificial dissipation scaling.

Figures 6 and 7 show the influence of this treatment. With the reduced viscosity $D(w)$, steeper gradients occur at the separation, which agrees better with the experiment. The point of separation is unaffected. Again, it should be underlined that the used matrix dissipation is already less dissipative than the scalar one. We have also tried a TVD sensor for this case but got no significant improvements. Figure 2 shows experimental values for the pressure in front of the separation that seem to be too high in comparison with our

Table 1 Flow conditions for He injection test case

	Helium jet	Air mainstream
p, bar	12.4	0.663
T, K	217	108
Ma	1	2.9
Y_{He}	1	0
Y_{N_2}	0	0.7664
Y_{O_2}	0	0.2336

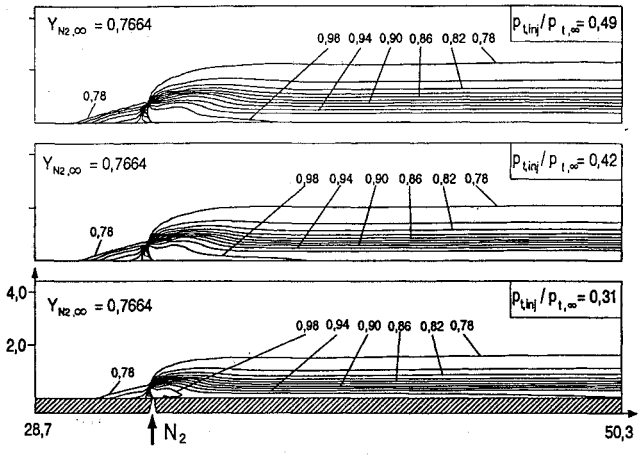

Fig. 8 Lines of constant nitrogen mass fractions.

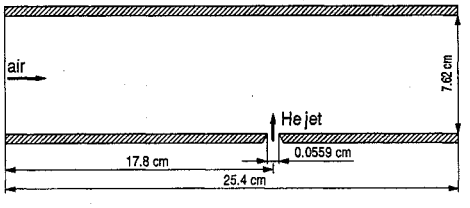

Fig. 9 Geometry for He injection test case.

and other[16,19] calculations. Clark and Chan[19] found from flat plate compressible flow theory a value of $p_{Wall}/p_\infty = 1.005$ that would be in good agreement with our numerical result.

In another investigation we have varied the turbulence intensity of the nitrogen jet between $Tu_{inj} = 0.005$ and 0.1 without getting visible differences. Results for increased pressure ratios $p_{t_{inj}}/p_{t_\infty} = 0.42$ and 0.49 also show a good overall agreement with the experiment.[20] Finally, the nitrogen distributions for all investigated pressure ratios are given in Fig. 8.

Helium Wall Injection

The second wall jet experiment considered was conducted by Kraemer and Rogers and is reported by Weidner and Drummond.[21] The geometry of this experiment is given in Fig. 9. The flow is assumed to be turbulent throughout. The computational grid consists of 232 × 96 grid points, and 15 grid points are used for the injection slot. The inflow conditions for the air and the sonically injected helium are given in Table 1. In addition to the surface wall pressure given in Fig. 10, the cross-stream pressure (Fig. 11), has been measured and is compared with theoretical results. The injector is located at $x = 0$. The computational results upstream of the injector compare reasonably well with the experimental data. However, the leading separation bubble is smaller than in the experiment. Downstream of the injector the pressure is to some extent overpredicted. Especially the peak, which occurs in experimental data at $x = 3$ cm, is not reproduced by the computation. These discrepancies may also cause the underprediction in peak pressure shown in Fig. 11 as well as its shift towards the lower wall. For this experiment helium mass fractions have been measured for the same cross section. Figure 12 shows a comparison between the numerical and experimental results.

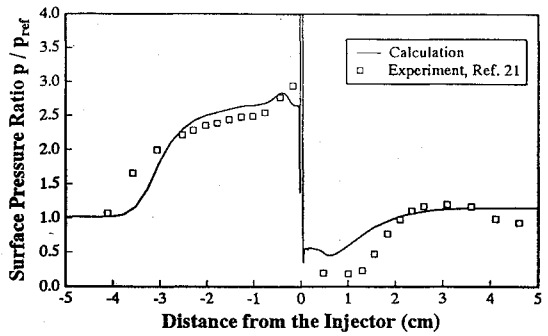

Fig. 10 Surface static pressure distributions (p_{ref} = 0.66323 bar).

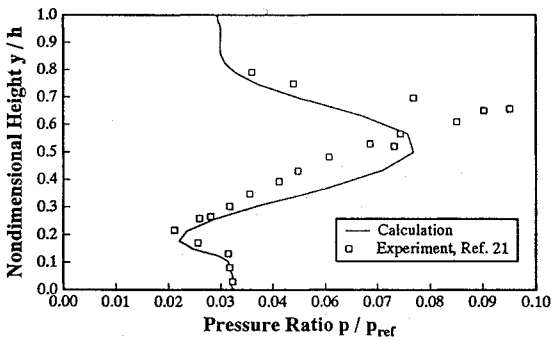

Fig. 11 Cross-stream static pressure distributions at x = 3.81 cm (p_{ref} = 21 bar).

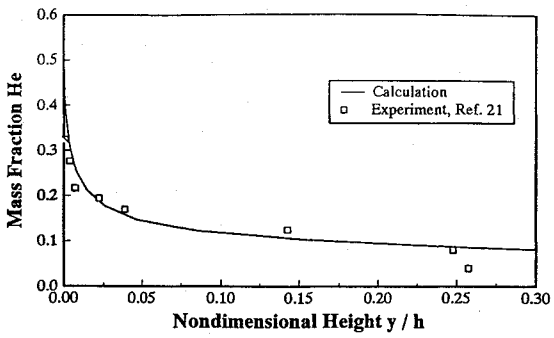

Fig. 12 Helium mass fraction distributions at x = 3.81 cm.

Burrows–Kurkov Mixing Experiment

The third wall jet experiment considered was conducted by Burrows and Kurkov[22] and investigates axial hydrogen injection. The geometry of the test section, which is identical to the computed field, is given in Fig. 13. The computational grid consisted of 2 blocks with 99 × 57 and 119 × 75 grid points. The boundary line that separates the two blocks is the nearly horizontal line plotted in Fig. 14 . The grid resolves the lip above the injector, which has a strong influence on the flow pattern. The high temperature gas stream for this experiment is produced by precombustion that is performed in such a way that no oxygen and only a small fraction of hydrogen is left in the test section. The conditions for the vitiated airstream and the sonically injected hydrogen are shown in Table 2. We started the calculation 2 cm upstream of the wall step where we assumed fully turbulent inlet profiles for u, T, q, and ω. However, because of the inflow setting $v = 0$, weak shocks are formed that may be observed in the pressure distributions given in Figs. 14 and 15. The boundary-layer thickness of 1.2 cm is known from experiment. The first out of two calculations with matrix dissipation is performed with the original pressure-based sensor, whereas for the second calculation the TVD sensor is used. At the corner of the wall step an expansion fan is formed that is followed by a shock wave. The oscillations in front and behind of this shock are reduced by the TVD sensor. On the other hand this sensor is more dissipative than the original one. Because the hydrogen is injected parallel to the mainstream, supersonic mixing is dominated by turbulent diffusion. This is in contrast to the previous cases, where the injection pressure has a strong influence on the penetration depth and the mixing process. The mole fraction distributions of H_2, N_2, and H_2O for the cross section 35.6 cm downstream of the injector are plotted in Fig. 16. Theoretical and experimental results compare very well in the near-wall region of the mixing zone ($y \leq 0.7$ cm). With growing distance from the wall the calculated profiles are steeper than those of the experiment. Similar observations are made for the same test case including combustion.[10] Improvements could be achieved by using smaller turbulent Schmidt numbers than 0.9. Libby and Williams[23] reported that for binary mixtures of gases with large and small molecular weights the turbulent Schmidt number may be as low as 0.25. However, the use of lower values would require new experiments to determine turbulent Schmidt numbers depending on the molecular weights of the different species.

Table 2 Flow conditions for H_2 injection test case

	Hydrogen	Air mainstream
p, bar	1.0	1.0
T, K	254	1150
Ma	1.0	2.44
X_{H_2}	1	0.011
X_{N_2}	0	0.672
X_{H_2O}	0	0.317

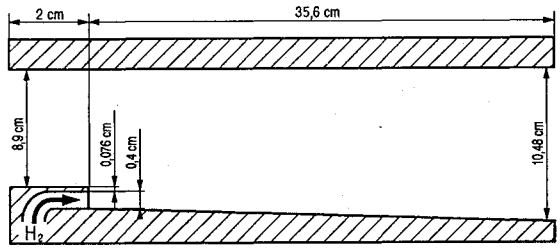

Fig. 13 Geometry for Burrows–Kurkov experiment.

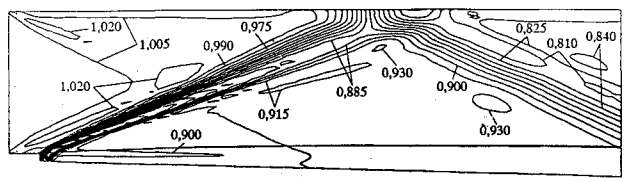

Fig. 14 Calculated pressure distribution using matrix dissipation.

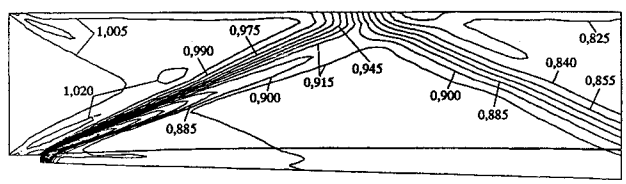

Fig. 15 Calculated pressure distribution using TVD matrix dissipation.

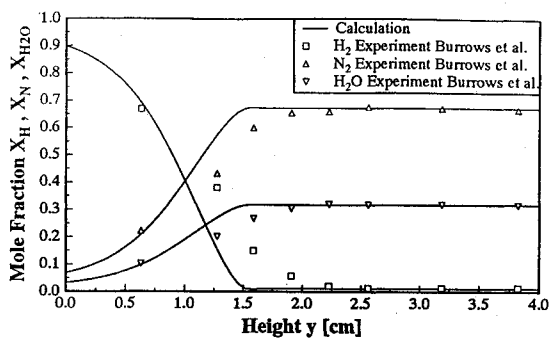

Fig. 16 Composition profiles at x = 35.6 cm.

Conclusions

We have investigated the influence of different modeling corrections for a low-Reynolds-number q-ω turbulence model. The combination of the described corrections 1 and 2 leads to the best overall agreement with experiments. Further improvements could be achieved by a reduction of the added artificial viscosity in the near wall-region. The q-ω model has proven to be very stable even in cases with wall injection, high total pressure ratios, and massively separated flow.

Acknowledgment

We wish to thank the Deutsche Forschungsgemeinschaft (DFG) for financial support of this work within the SFB 259 at the University of Stuttgart.

References

[1]Coakley, T. J., and Huang, P. G., "Turbulence Modeling for High Speed Flows," AIAA Paper 92-0436, Jan. 1992.

[2]Gerlinger, P., and Algermissen, J., "Numerical Calculation of Supersonic Combustion Problems Using an Implicit LU-SGS Scheme and k-ϵ/q-ω Turbulence Closure," AIAA Paper 93-5021, Dec. 1993.

[3]Launder, B. E., and Sharma, B. I., "Application of the Energy Dissipation Model of Turbulence to the Calculation of Flows near a Spinning Disk," *Letters in Heat and Mass Transfer*, Vol. 1, No. 2, 1974, 131–138.

[4]Shuen, J. S., and Yoon, S.,"Numerical Study of Chemically Reacting Flows Using a Lower-Upper Successive Verrelaxation Scheme," *AIAA Journal*, Vol. 27, No. 12, 1989, pp. 1752–1760.

[5]Yoon, S., and Jameson, A., "An LU-SSOR Scheme for the Euler and Navier–Stokes Equations," AIAA Paper 87-0600, Jan. 1987.

[6]Shuen, J. S., "Upwind Differencing and LU Factorization for Chemical Non–Equilibrium Navier–Stokes Equations," *Journal of Computational Physics*, Vol. 99, No. 2, 1992, 233–250.

[7]Jameson, A., Schmidt, W., and Turkel, E., "Numerical Solution of the Euler Equations by Finite Volume Methods Using Runge–Kutta Time Stepping Schemes," AIAA Paper 81-1259, June 1981.

[8]Turkel, E., "Improving the Accuracy of Central Difference Schemes," NASA CR 181712, Sept. 1988.

[9]Swanson, R. C., and Turkel, E., "On Central Difference and Upwind Schemes," NASA CR 182061, June 1990.

[10]Gerlinger, P., Algermissen, J., and Brüggemann, D., "Numerical Solutions of Supersonic Combustion Problems with TVD-Matrix Dissipation," AIAA Paper 94-3181, June 1994.

[11]Kunz, R. F., and Lakshminarayana, B., "Explicit Navier–Stokes Computation of Cascade Flows Using the k-ϵ Turbulence Model," *AIAA Journal*, Vol. 30, No. 1, 1992, pp. 13–22.

[12]Coakley, T. J., "Turbulence Modeling Methods for the Compressible Navier–Stokes Equations," AIAA Paper 83-1693, July 1983.

[13]Coakley, T. J., and Hsieh, T., "A Comparison Between Implicit and Hybrid Methods for the Calculation of Steady and Unsteady Inlet Flows," AIAA Paper 85-1125, July 1985.

[14]Vuong, S. T., and Coakley, T. J., "Modeling of Turbulence for Hypersonic Flows with and without Separation," AIAA Paper 87-0286, Jan 1987.

[15]Sarkar, S., Erlebacher, G., Hussaini, M. Y., and Kreiss, H. O., " The Analysis and Modeling of Dilatational Terms in Compressible Turbulence," NASA CR181959, Dec. 1989.

[16]Rizzetta, D. P., "Numerical Simulations of Slot Injection into a Turbulent Supersonic Stream," *AIAA Journal*, Vol. 30, No. 10, 1992, pp. 2434–2439.

[17]Aso, S., Okuyama, S., and Kawai, M., "Experimental Study on Mixing Phenomena in Supersonic Flows with Slot Injection," AIAA Paper 91-0016, Jan. 1991.

[18]Wallin, S., and Gronland, T., "CFD Investigations on the Hypersonic Double Delta Wing Greta," AIAA Paper 93-5064, Dec. 1993.

[19]Clark, S. W., and Chan, S. C., "Numerical Investigation of a Transverse Jet for Supersonic Aerodynamic Control," AIAA Paper 92-0639, Jan. 1992.

[20]Gerlinger, P., Algermissen, J., and Brüggemann, D., "Simulation of Turbulent Slot Injection of Different Gases into a Supersonic Air Stream," AIAA Paper 94-2247, June 1994.

[21]Weidner, E. H., and Drummond, J. P., "Numerical Study of Staged Fuel Injection for Supersonic Combustion," *AIAA Journal*, Vol. 20, No. 10, 1981, pp. 1426–1431.

[22]Burrows, M. C., and Kurkov, A. P., "Supersonic Combustion of Hydrogen in a Vitiated Air Stream Using Stepped-Wall Injection," AIAA Paper 71-721, June 1971.

[23]Libby, P. A., and Williams, F. A., "Fundamental Aspects," *Turbulent Reacting Flows*, edited by P. A. Libby and F. A. Williams, Springer–Verlag, Berlin, 1980, p. 5.